Assessment of the environmental sustainability of solvent-less fatty acid ketonization to bio-based ketones for wax emulsion applications

Bert Boekaerts[a], Margot Vandeputte[a], Kranti Navaré[b,c], Joost Van Aelst[a], Karel Van Acker[b,d], Jan Cocquyt[e], Chris Van Caneyt[e], Peter Van Puyvelde[f] and Bert F. Sels[a]

a. Department of Microbial and Molecular Systems (M²S), Centre for Sustainable Catalysis and Engineering (CSCE), KU Leuven, Celestijnenlaan 200F, 3001 Leuven, Belgium.

b. Department of Materials Engineering, KU Leuven, Kasteelpark Arenberg 44 box 2450, BE-3001 Leuven, Belgium.

c. Unit Sustainable Materials, VITO, Boeretang 200, 2400 Mol, Belgium.

d. Center for Economics and Corporate Sustainability (CEDON), KU Leuven, Warmoesberg 26, BE-1000 Brussels, Belgium.

e. GOVI NV, Landegemstraat 8, 9031 Drongen, Belgium.

f. Department of Chemical Engineering, KU Leuven, 200F, B-3001, Heverlee, Belgium

E-mail: bert.sels@kuleuven.be

Supporting information

Experimental

1. Life Cycle Assessment

Datasets and detailed descriptions.

Paraffin wax. The GaBi dataset "Wax / Paraffins at refinery; from crude oil; production mix, at refinery; 38 MJ/kg net calorific value (en)" has been chosen for the benchmark LCAp.[1] This refining process is well-known, though variable and complex. The refinery setup strongly depends on the location of the plant, the composition and origin (red. quality) of the crude oil, the used electricity mix, etc. To generate the energy needed for a refinery plant, various fuels originating from the refinery plant itself (refinery gas, heating oil, petroleum coke etc.) are burnt and, in addition, purchased natural gas and electricity are used. All these forms of energy are modelled consistent with the scenario specific for the European Union (EU-28), taking the particular EU emission standards and energy carriers into account. With respect to the corresponding energy carrier input, efficiencies for thermal energy production of 100% are defined. For process steam the efficiency varies from 85% to 95%. Almost every refinery unit process has the same inputs, namely thermal energy, steam, electricity and crude oil (only fed as such in the atmospheric distillation unit, the other unit processes consume a corresponding amount of crude oil). The distribution of the environmental impacts of these inputs are distributed with different allocation factors. The emissions from the refinery itself are all assumed to come from the refinery power plant. These emissions are allocated to the different unit processes according to their energy consumption. This assumption is justified given that 95% of the refinery emissions are coming from the on-site power plant. In this GaBi refinery model, both mass and economic allocation are applied. The refinery

emissions, natural gas and external electricity are allocated by mass, while the impacts from crude oil supply are allocated by calorific content. The impacts of hydrogen and methanol/ethanol supply are allocated to the related end-products. Overall, the allocation condition must always be met: the sum of the allocated inputs and outputs of a unit process must be equal to the sum of the original, non-allocated inputs and outputs.

PFAD. For the production of refined palm oil, the aggregated Gabi process data set "MY Palm oil, refined; technology mix; production mix, at plant; refined (incl. LUC as fossil CO_2)" is used.[2] This dataset is representative for the country of Malaysia (MY). In this study, PFAD is first transported by cargo ship from Pasir Gudang port, one of major palm oil export ports in Malaysia to the port of Rotterdam.[3] This transport process is modelled by using the parametrized GaBi thinkstep process for an ocean going oil tanker (global average) of 10 000 to 300 000 ton dry weight payload capacity. The heavy fuel (1wt% of S) consumption is included and calculated on the basis of the port-to-port distance of 15 396 km.[4] Once the PFAD has arrived in the port of Rotterdam, it will be transported further by a diesel-powered truck to Belgium. The truck's diesel consumption is calculated based on a port-to-destination distance of around 170 km. Most of the palm oil and PFAD imported in the European Union (the geographical boundary of this LCA_b) is produced in Malaysia. It is the world's second largest palm oil producer (after Indonesia) and is the leading exporter to the European Union.[5] Belgium imports most of its palm oil from Malaysia, of which 8.1% is directly imported via the port of Antwerp.[6] The majority (76%) of the palm oil in Belgium is imported from the Netherlands where ships from predominantly Indonesia (34%) and Malaysia (20%) arrive in the port of Rotterdam, the number one import port for palm oil in Europe.[7] This justifies the choice for Malaysia as a representative production location for the PFAD feedstock for LCA_b. The used GaBi dataset on the production of refined palm oil is based on the latest literature and the overall data quality is classified as very good by Thinkstep's data quality indicators system. The most important assumptions of this dataset are listed as follows. The system boundary is defined as cradle-to-gate and thus includes the cultivation (cradle) of the palm oil bearing fresh fruit bunches (FFB) and all the subsequent processing steps required to reach the gate of the dataset (refined palm oil). An average yield of 20.7 tons of FFB per hectare per year over a cultivation period of 25 years is presumed. Once ripe, the FFB are harvested by hand every 10 to 15 days and left at the side of the road to be transported by lorry to the palm oil mill, where the oil winning process is taking place. First, the FFB are sterilized and threshed to free the palm fruits. These fruits are then mashed after which the crude oil is pressed out. This crude oil is further treated and purified to obtain the desired refined palm oil. More specifically, it undergoes degumming, bleaching and deodorization processes during the refining step to obtain desirable colour, odour and taste for the final refined palm oil (RPO). The degraded volatile fats and free fatty acids present in the crude oil are hereby removed from the RPO by distillation and this fraction is obtained as the PFAD by-product after condensation (4-5 wt%).[8] In this dataset, all relevant and identified transport processes are taken into account. Furthermore, electricity and thermal energy (process steam) are modelled according to the specific situation of Malaysia in line with national emission standards and energy carriers. To divide the environmental burdens between the different by-products, economic allocation with prices from the World Bank, the Malaysian Palm Oil Board and FAOSTAT has been chosen for the base case scenario. The by-products include the Empty Fruit Bunches (EFB) from threshing, Press Cake (Palm Kernels (PK)) from oil extraction, Palm Oil Mill Effluent (POME) from purification and Palm Fatty Acid Distillate (PFAD) from refining. The POME is treated in anaerobic open ponds leading to methane and other emissions (N_2O and NH_3). In the GaBi dataset, it is assumed that 5% of these methane emissions is captured for energy recovery. At the time of writing, PFAD is being sold at a price worth 78% of the market value of refined palm oil. Finally, this GaBi process includes the impact of land use change (LUC) as fossil carbon dioxide. Based on data concerning the change of land use of forests and plantations, the area which was subject to land use change has been calculated. It is assumed that 43% of the current

area of palm plantations was known to be natural forest before 1990. The direct land use change emissions occurring from the deforestation of this area are accounted with 29.4 kg of CO_2 per hectare per year.[9] Land area which was already converted before 1990 is not assigned any land use change emissions.

TiO_2. Commercially, TiO_2 is produced by either a chloride or sulphate process. The latter is chosen in this study since the catalysts used in this work originate from the sulphate process, which is also the most common production technology in Europe. The sulphate process starts from ilmenite ($FeTiO_3$) or "titania slag", which is an iron extraction residue of ilmenite ore. These raw materials are first dissolved in strong sulphuric acid at 100 °C, leading to a mixture of titanyl ($TiOSO_4$) and iron sulphates ($FeSO_4$). Next, a hydrolysis step at 110 °C causes selective precipitation of hydrated titanium dioxide. The final step is a calcination treatment at 650-1000 °C to remove water and obtain the correct crystallization towards rutile or anatase phase.[10]

Results and discussion

1. Catalyst Characterization

PXRD. Via powder X-ray diffraction (PXRD), it was found that the catalysts exclusively contain an anatase crystal phase structure with (101) as the main surface (highest signal intensity at 2 theta values around 25-26 degrees), while no reflections of rutile crystal phase are observed (Figure S1). Other crystallographic surfaces are present in minor amounts: (112), (200) and (211), respectively. Furthermore, primary crystallite sizes were of 9.6 and 7.8 nm were determined for KK7500 and HM211 via the Scherrer equation, respectively. This is in good agreement with the product specifications provided by the manufacturers, which state that the primary crystal sizes vary between 5-15 nm.

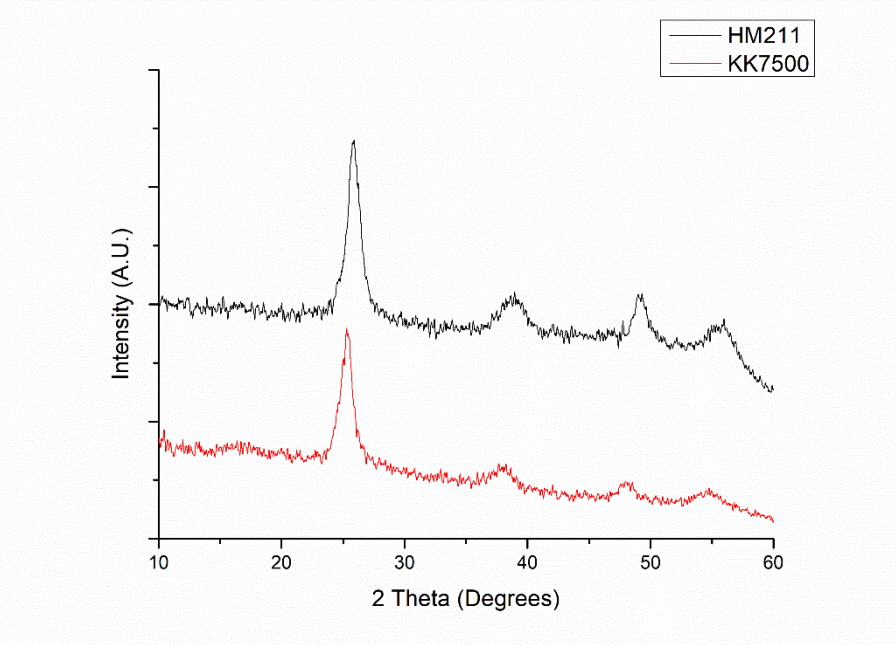

Figure S1: Powder XRD analysis of HM211 and KK7500 TiO_2 catalysts.

DRS UV-vis. The DRS UV-vis measurements confirm the sole presence of the anatase crystal phase as band gap energies of ~3.25-3.3 eV were found using the Kubelka-Munk theory for both materials (Figure S2). These are typical values reported in literature for anatase TiO_2, while the band gap of rutile TiO_2 is typically lower around 3.0-3.1 eV.[11]

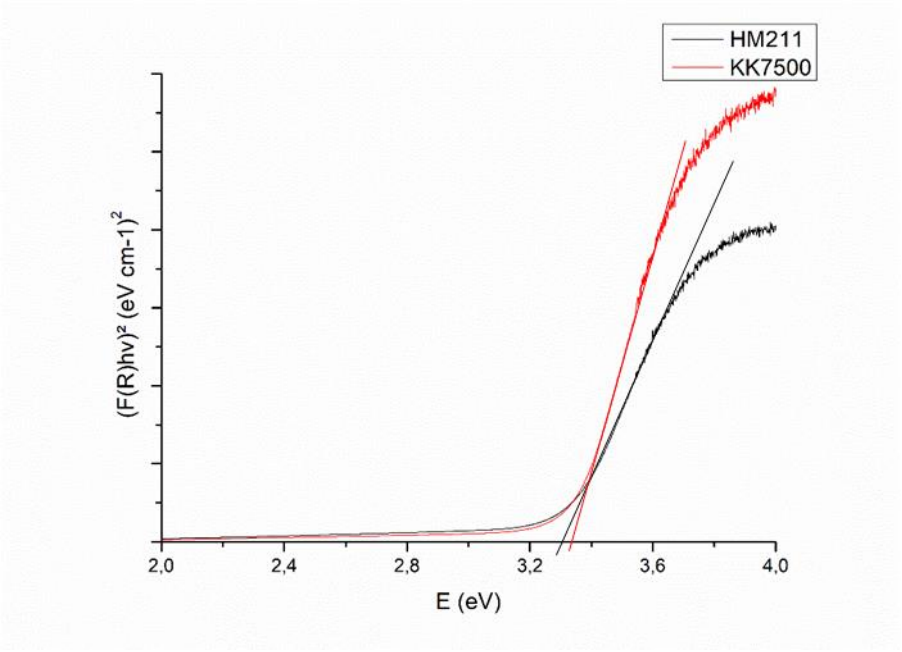

Figure S2: DRS UV-vis characterization of HM211 and KK7500 TiO_2 catalysts with Kubelka-Munk theory analysis.

SEM. Scanning electron microscopy (SEM) images show for both catalysts that the primary crystallites are aggregated into larger heterogeneously sized particles of up to 50 µm (Figure S3).

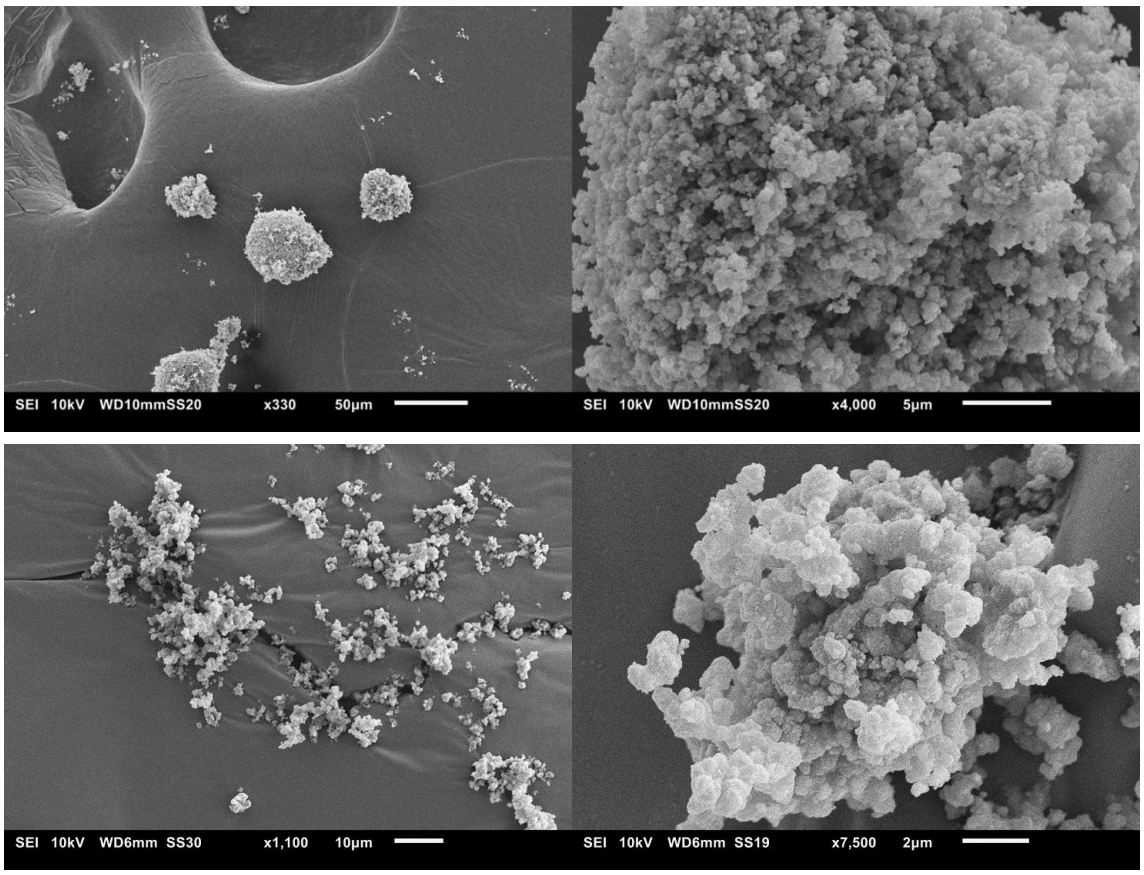

Figure S3: Scanning electron microscopy images of HM211 (top) and KK7500 (bottom) TiO_2 catalysts.

N_2 physisorption. Via the N_2 physisorption isotherms, BET surface areas of 248 and 266 m²/g were measured for KK7500 and HM211, respectively (Figure S4).

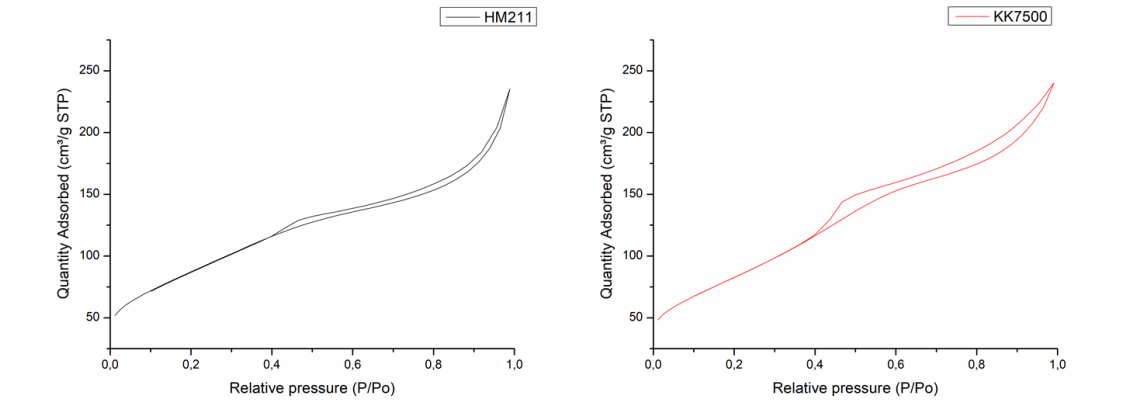

Figure S4: Nitrogen physisorption isotherms of HM211 (left) and KK7500 (right) TiO_2 catalysts.

NH_3-TPD. The acidic properties of the TiO_2 catalysts were first investigated via temperature programmed desorption (TPD) with NH_3 as probe molecule. The broad signals were deconvoluted to distinguish between acid sites with different acid strength, after normalizing the signal intensities for the catalyst mass and surface area (Figure S5). For KK7500, deconvolution (R^2=0.999) showed a first peak maximum at 242°C, indicating the presence of weaker acid sites (16% of the total signal area), while the second maximum at 324°C may be attributed to the presence of medium strength acid sites (53%). Stronger acid sites are also detected at desorption peak temperatures of 440 (26%) and 595°C (5%) respectively, constituting the remaining part of the total amount of acid sites. For HM211, deconvolution (R^2= 0.999) resulted in three curves with peak maxima at 240, 319 and 422 °C, attributed to weak (17%), medium (56%) and strong acid sites (27%), respectively. The slightly lower desorption temperatures of the peak maxima for HM211 and the absence of very strong acid sites compared to KK7500 indicate a lower acid site strength. Quantitatively, the total signal area for KK7500 is 1.22 times higher than for HM211 after normalization, also revealing a higher total acid site density.

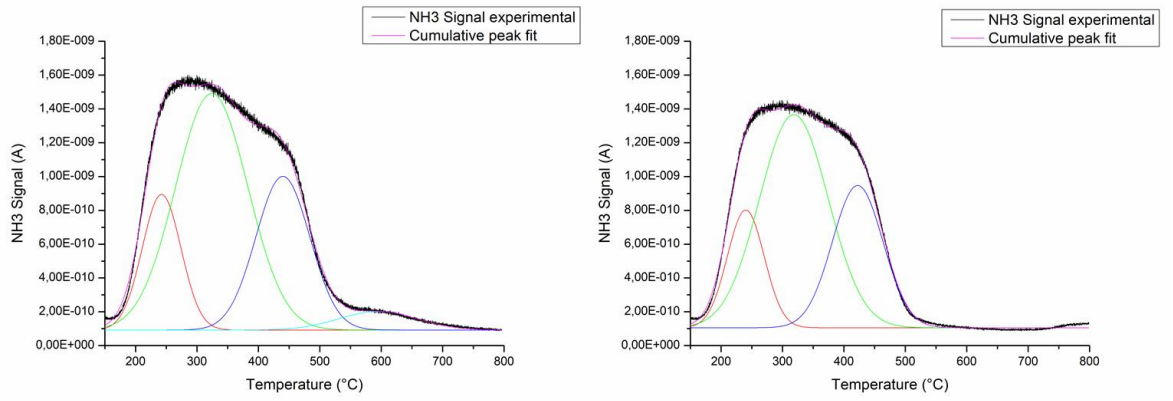

Figure S5: NH_3-TPD measurement with deconvolution analysis of KK7500 (left) and HM211 (right).

Pyridine FT-IR. To distinguish between the presence of Lewis and Brönsted acid sites, pyridine FT-IR spectroscopy was measured. For KK7500, absorption bands at 1445, 1492, 1575 and 1606 cm^{-1} were observed, while no Brönsted acid sites (situated at wavenumber values of 1545 and 1635 cm^{-1}) were detected (Figure S6). Quantification of these measurements was performed by integration of the absorption band at 1445 cm^{-1} using an extinction coefficient value of 1.63 for the Lewis acid sites of TiO_2.[12, 13] For this material, the acid site density values after desorption at 150, 250 and 350 °C were 2.17, 1.29

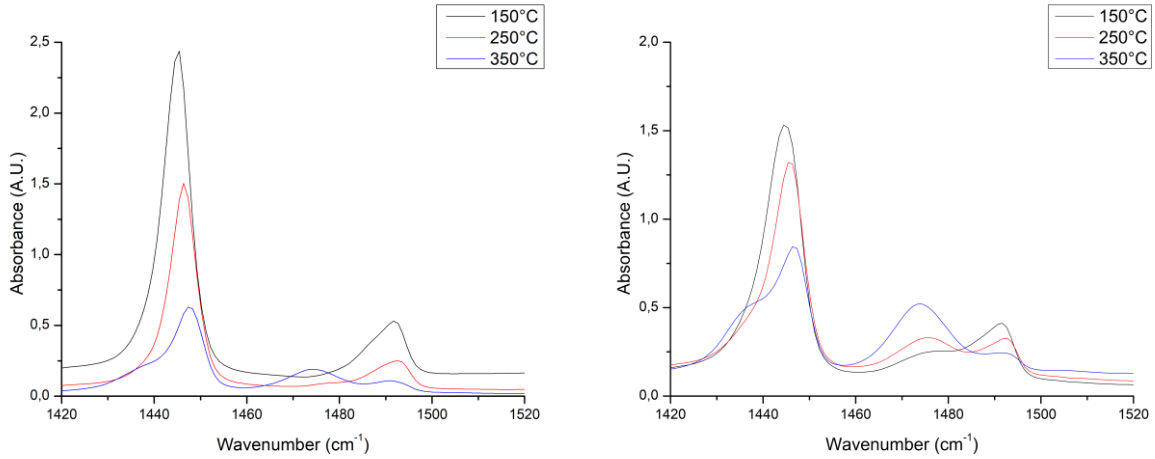

Figure S6: Pyridine FT-IR measurement after different desorption temperatures for KK7500 (left) and HM211 (right).

and 0.52 μmol/m² respectively, indicating the presence of Lewis acid sites with varying acid site strength. This is also evidenced by the minor shift in absorption wavenumbers as function of the desorption temperature. Similarly, HM211 showed Lewis acid absorption bands, while no Brönsted acid sites were detected. For this catalyst material, the acid site density values at 150, 250 and 350 °C were 1.22, 0.86 and 0.42 μmol/m², respectively, indicating the lower amount of Lewis acid sites compared to KK7500.

CO_2-TPD. The base properties were studied via TPD with CO_2 as probe molecule, after normalizing for the catalyst mass and surface area (Figure S7). For KK7500, CO_2-TPD shows a large amount of weak basic sites with desorption peak temperatures at 97 °C (81% of total signal area) and 122 °C (16%) after deconvolution (R^2=0.998). Additionally, a very small amount of (very) strong basic sites were observed between 400-700 °C with peak maxima at 520 °C (2%) and 613 °C (1%), respectively. For HM211, two broad signals between 50-225 °C and 425-800 °C were observed which can be assigned to weak and strong basic sites, respectively. After deconvolution (R^2= 0.998) 5 peak maxima were obtained at 85 °C (30%) , 105 °C (40%), 515 °C (5%), 634 °C (14%) and 736 °C (11%). These data indicate a stronger basicity for the HM211 catalyst, while integration of the total CO_2 signal revealed that the total basic site density measured by TPD is 4.20 times higher for HM211 compared to KK7500 after normalization.

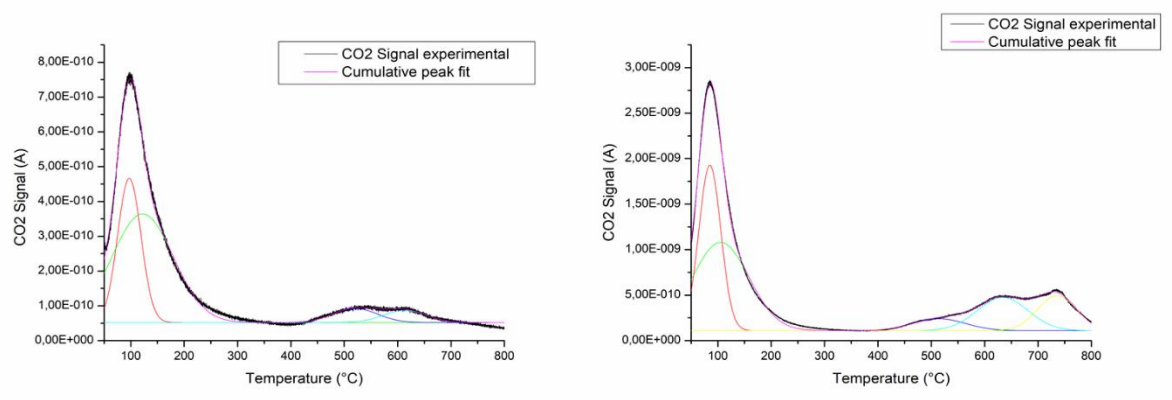

Figure S7: CO_2-TPD measurement with deconvolution analysis of KK7500 (left) and HM211 (right).

2. Fatty acid ketonization

Ketonization pressure in batch reactor. Visualization of increase in autogenous pressure during the ketonization reaction of stearic acid in a batch reactor (Figure S8). At 340°C, CO_2 and H_2O formation result in a pressure increase, the evolution of which is dependent on the stearic acid conversion rate. We have also carried out a reference stearic acid ketonization reaction where an initial N_2 pressure of 30 bar was applied. Compared to an initial pressure of 1 bar, there was no significant impact on the reaction rate.

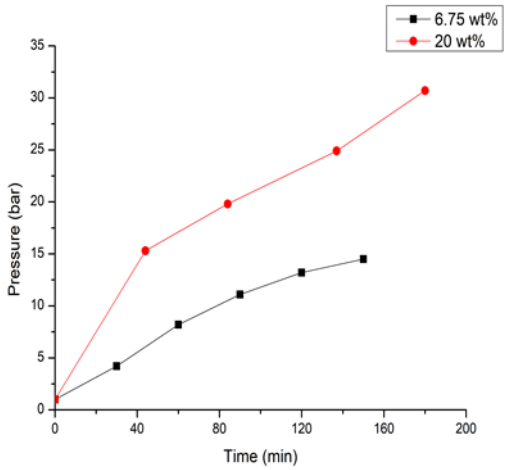

Figure S8: Autogenous reactor pressure as function of time and catalyst loading during batch ketonization reaction. m_{SA}= 40 g - KK7500 TiO_2 – 340 °C – 600 rpm.

Impact of semi-batch and N_2-flow on ketonization reaction. The activity of KK7500 TiO_2 was also investigated in semi-batch operation with a varying N_2-flow between 0-50 ml/min (Figure S9). In this case 0 ml/min for the semi-batch experiment ("0 (SB)") means that the reactor head space outlet towards the condenser cooling system was opened without applying an actual external N_2-flow.

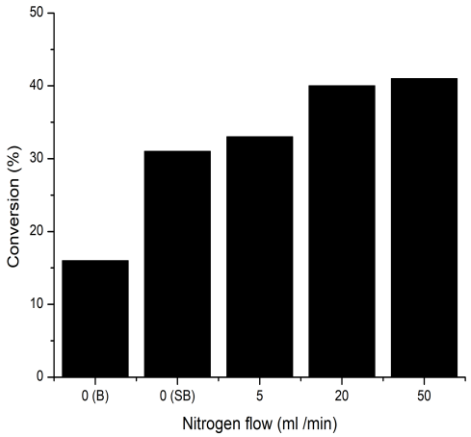

Figure S9: Comparison between batch (B) and semi-batch (SB) experiments with varying N_2-flow. m_{SA}=40 g - 6.75 wt% KK7500 – 340 °C - 2.5 h – 600 rpm - 5 bar.

Influence of reaction temperature on PFAD ketonization. The batch ketonization of PFAD was investigated between 300-350°C (Figure S10). As shown, an exponential relationship was observed between the ketonization temperature and PFAD conversion. For example, nearly 80% of the biomass substrate was converted at 350 °C under the applied process conditions, while only 14% was converted at 320°C. From these results, an apparent activation energy of 177 kJ/mol was obtained via the Arrhenius equation (R^2=0.999), after assuming a zero order reaction due to surface saturation of the active catalytic sites as pure substrate without any solvent or additive is used.

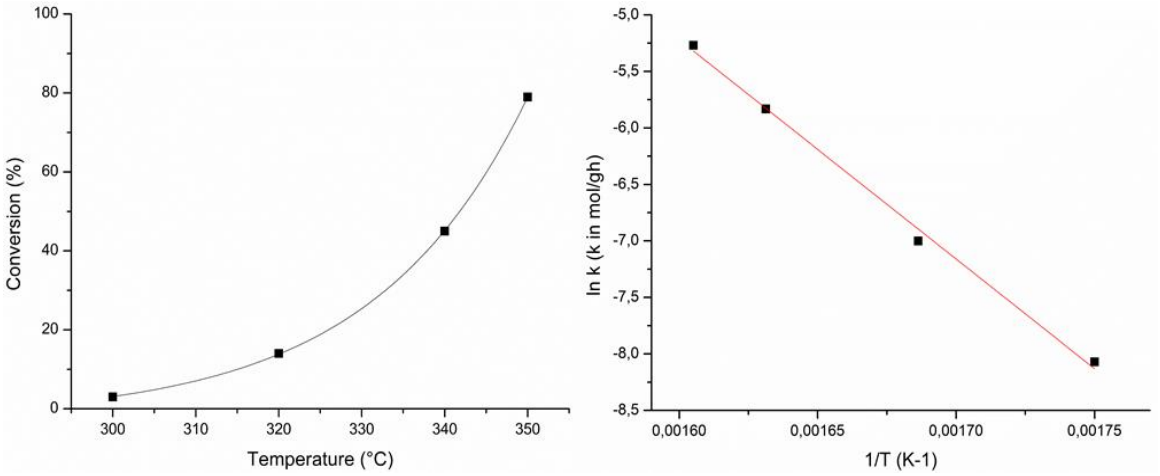

Figure S10: Exponential influence of reaction temperature on batch ketonization of PFAD (left). Determination of zero order apparent activation energy via Arrhenius plot (R^2=0.999) (right). m_{PFAD}= 40 g PFAD – 20 wt% KK7500 – 3 h – 600 rpm – autogenous pressure.

Catalyst stability. To test the catalyst stability, three consecutive runs were performed without any catalyst treatment between experiments (Figure S11). Separation of the solid active material was established in a heated centrifuge setup (100 °C) to ensure liquification of the substrate-product mixture. As shown in the graph, a decline in the catalytic activity of KK7500 was observed, which resulted in a 45% loss of initial activity after 2 reuses without

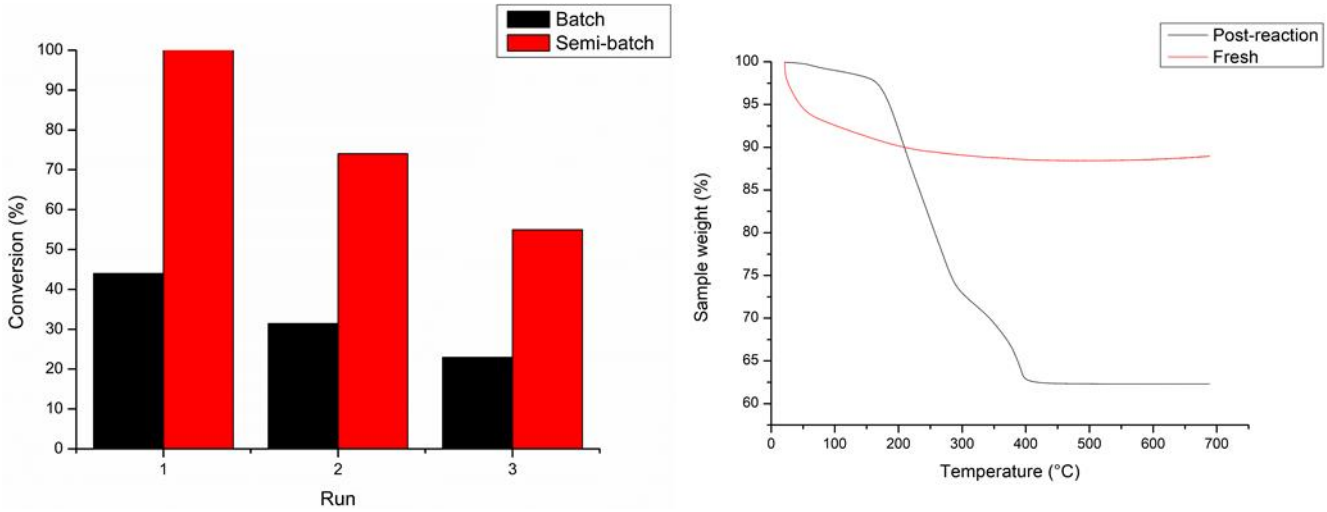

Figure S11: Catalyst re-use experiments for ketonization of PFAD in batch and semi-batch mode. Batch conditions: 20 wt% KK7500 – 340 °C – 3 h - 600 rpm – autogenous pressure. Semi-batch conditions: 5 wt% KK7500 – 350 °C – 6 h - 600 rpm – 5 ml/min N_2 at 5 bar (left). Fresh and post-reaction TGA analysis of KK7500 (right).

any treatment under semi-batch conditions. This value was 49% for the batch reactions. To determine its cause, post-reaction analysis of the catalyst after run 1 of an in duplo experiment was conducted via TGA and N_2-physisorption techniques. The TGA profiles after treatment of the active material in O_2 up to 700°C shows that weight loss occurs up to a temperature of 400°C. This can be attributed to both water and organic phase comprising unconverted fatty acids, ketone products and side products as TGA analysis of the fresh parent catalyst shows an initial 10 wt% water loss.

Based on these results, a calcination treatment was performed in air at 400°C for 3 hours to remove any organics before measuring N_2-physisorption (Figure S12). Compared to the original material, 76% of the BET surface area was lost (from 248 to 59 m^2/g). While no calcination procedure was performed between the catalyst re-use experiments, these results may possibly indicate that the loss of catalytic activity in consecutive runs without treatment may be attributed to the loss of active surface area (and sintering) of the KK7500 material under the applied process conditions.

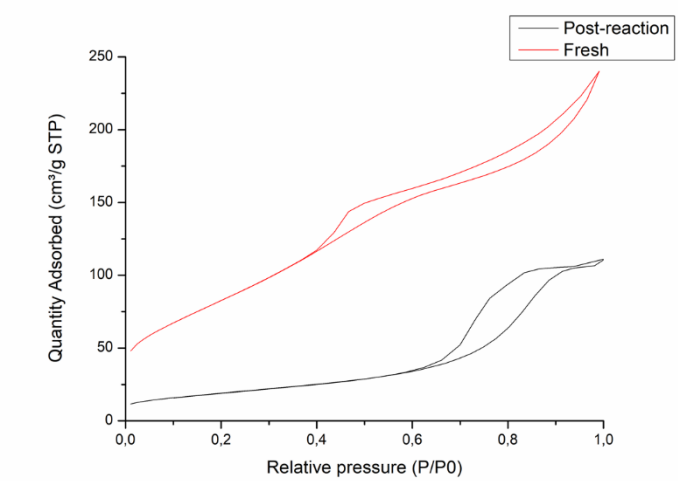

Figure S12: N_2 physisorption isotherms of fresh and post-reaction KK7500 TiO_2 after an air calcination treatment at 400°C for 3 hours after ketonization of PFAD.

3. Product analysis

PFAD hydrogenation and ketonization. Using a commercial hydrogenation catalyst (PRICAT Ni 52/35), the PFAD substrate was hydrogenated at 210 °C for 8 hours (30 bar H_2). The conversion of oleic and linoleic acid to stearic acid was nearly complete, with the hydrogenated PFAD containing a small amount (3 wt%) of residual oleic acid. This feedstock was then used as substrate for the ketonization reaction. After reaction under the base case conditions (99% conversion), a saturated bio-wax was obtained with a total ketone amount of 96%.

Gel Permeation chromatography – size exclusion. GPC-SEC analysis was performed to determine the potential presence of higher MW solid side products in the bio-wax samples. First, saturated C_{23}-C_{35} ketone standards (MW between 338-506 g/mol) were measured to determine their retention times (Figure S13 left). As expected, the higher MW ketones had a shorter retention time in the GPC column, showing a linear relationship between the MW and retention time of the peak maximum for the same class of molecules. Next, the retention times of palmitic acid (256 g/mol), oleic acid (282 g/mol), PFAD and a commercial hydrogenated C_{36} fatty acid dimer mixture (average MW around 562 g/mol) were also determined. A slight deviation from linearity between MW and peak retention time was observed by adding these compounds, indicating that not only molecular weight, but also size and chemical functionality (ketone, carboxylic acid) affects the interaction with the GPC column (Figure S13 right). Then, the GPC measurements of PFAD bio-waxes were compared to the hydrogenated counterpart, as well as the PFAD substrate and commercial dimer acid mixture (Figure S13 bottom). The PFAD bio-wax signal has a broad shoulder for retention

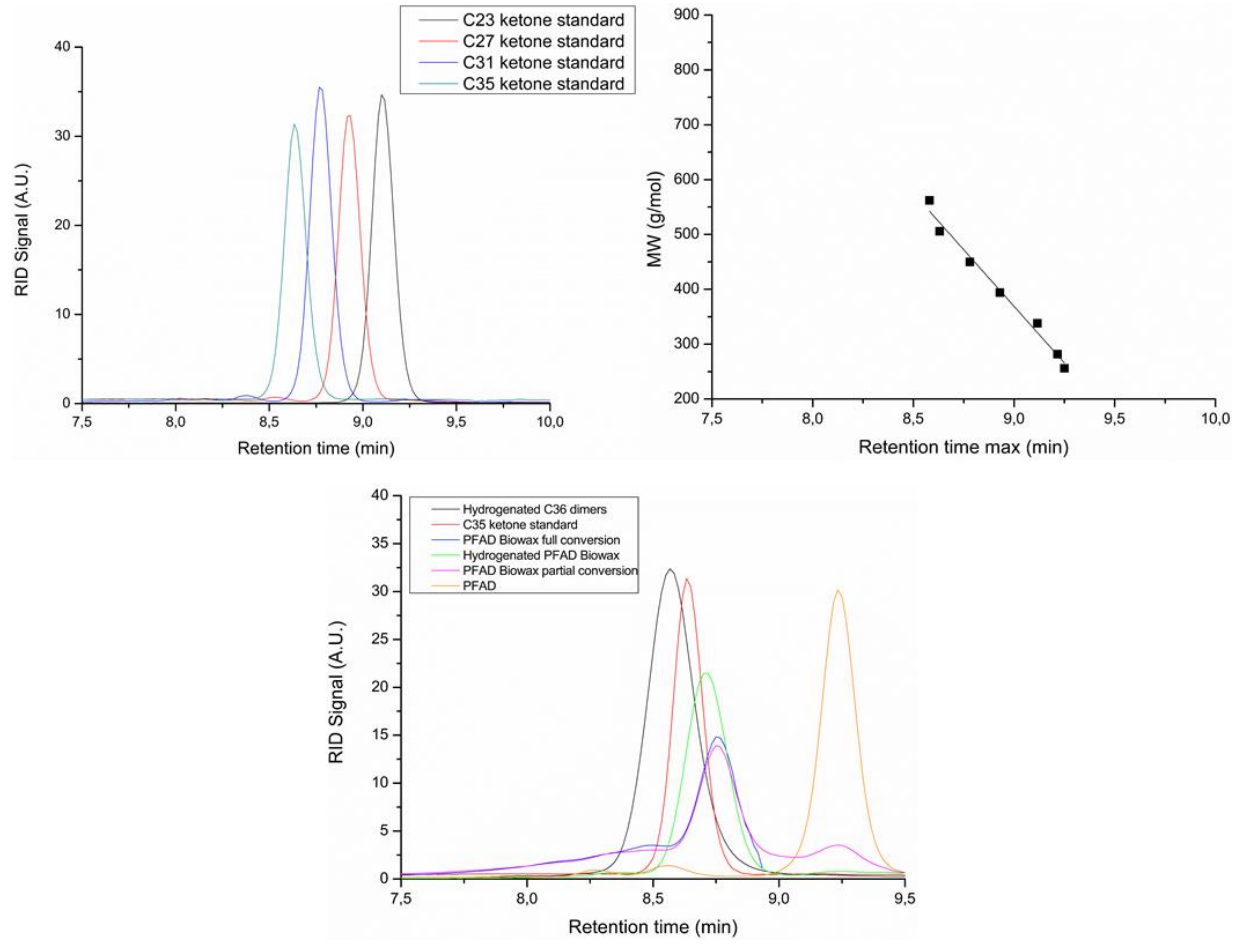

Figure S13: GPC-SEC measurements of reference C_{23}-C_{35} ketone standards (left); correlation between MW and GPC retention time (right); comparison between PFAD bio-wax samples and C_{36} hydrogenated dimer mixture (bottom).

times below 8.5 min., which is not present in the bio-wax originating from the hydrogenated PFAD substrate. This largely coincides with the elution of the C_{36} dimer sample, indicating the possible presence of unsaturated fatty acid dimers in the PFAD bio-wax. Additionally, it is well known that C_{54} fatty acid trimers are also formed during thermal/catalytic oligomerization of unsaturated fatty acids (Figure S14). These latter compounds have a MW around 840 g/mol. Extrapolating the relationship between MW and retention time in Figure S13 predicts a retention time peak around 7.9 minutes for a MW of 840 g/mol, which coincides with the onset of elution for the PFAD bio-wax signal. In general, the signal broadening is caused by the nature of the complex mixture containing linear, cyclic and aromatic unsaturated dimer and trimer compounds with slightly varying molecular weights, functionality and sizes. Note that some of the primary unsaturated C_{31}-C_{35} ketones may also undergo a secondary C=C coupling reaction with remaining unsaturated fatty acids, generating C_{49}-C_{53} keto-acid compounds with MW ranging between approximately 732-788 g/mol (estimated maximum peak retention times 8-8.2 min.). These can be regarded as a second type of trimers, as they also originate from C-C coupling of three fatty acid molecules (Figure S14). Integration of the signal area of higher MW compounds (> 506 g/mol) for the bio-wax sample revealed that it contributes 23% to its total signal area, which is in excellent agreement with the 24% unknown solid side products based on GC(-MS) analysis.

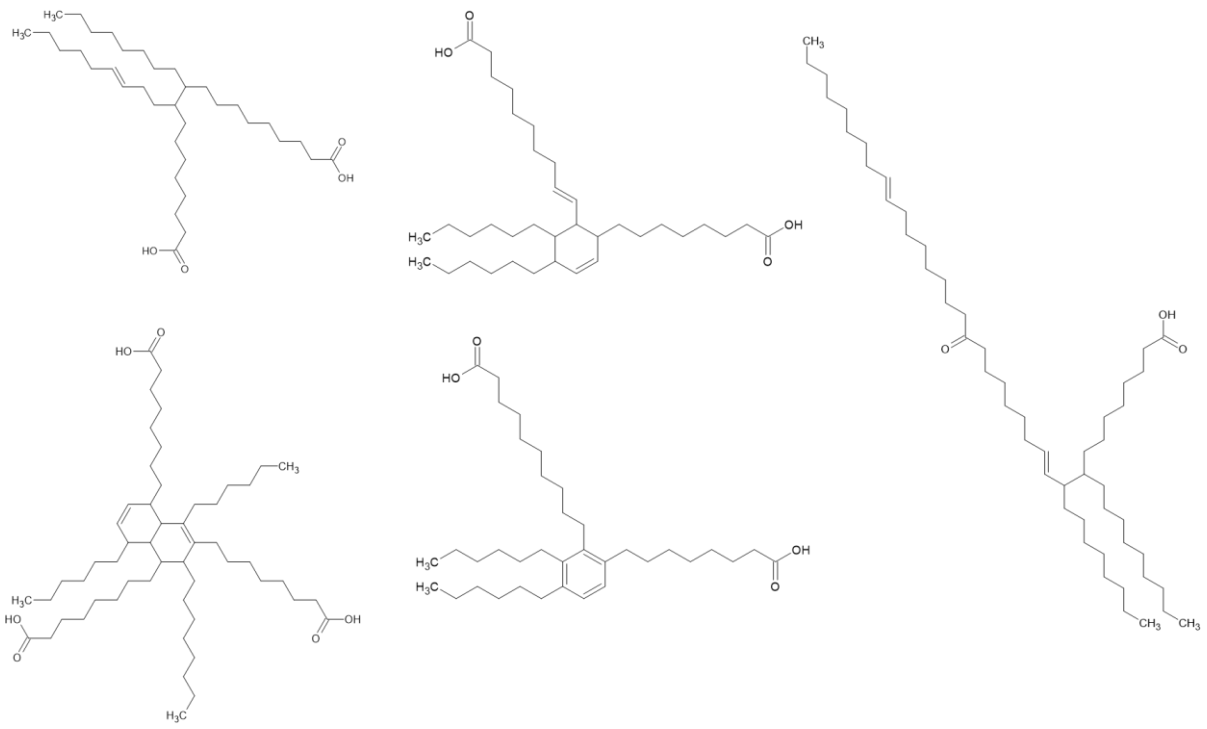

Figure S14: Possible fatty acid dimer, trimer and keto-acid structures including unsaturated linear, cyclic and aromatic compounds.

^{1}H-NMR. To further confirm the presence of dimers/trimers, the composition of the PFAD bio-wax was analysed via ^{1}H-NMR (Figure S15). The spectrum is complex, occasionally showing broad signals due to the presence of a multitude of different geometrical and positional C=C isomers, impacting the chemical shifts. Therefore, close up spectra are also shown in specific chemical shift regions because individual signals related to specific molecules might be small due to their low absolute amount in the wax sample. The presence of unsaturation in the PFAD bio-wax is evidenced by the broad signal around δ= 5.3-6.0 ppm for vinylic protons and around 1.9-2.1 ppm for allylic protons. As the unsaturated fatty acids have been fully converted, these are present in the main target ketones, as well as the dimer/trimer unsaturated side products. The ketone functionality is evidenced by the large multiplet around δ = 2.4 ppm. A triplet would be expected for the ketone compounds, but here the additional presence of carboxylic acid functionality is observed, further evidencing the presence of the dimer/trimer side products. Indeed, only a ketone triplet is observed in this region for the bio-wax originating from the hydrogenated PFAD substrate, as no fatty acid or fatty acid dimers/trimers are present in that sample. Furthermore, multiple small peaks around δ = 7 ppm are observed, showing the presence of aromatic compounds. Benzylic protons are also present, showing as small shoulder signals around 2.5 ppm.[14]

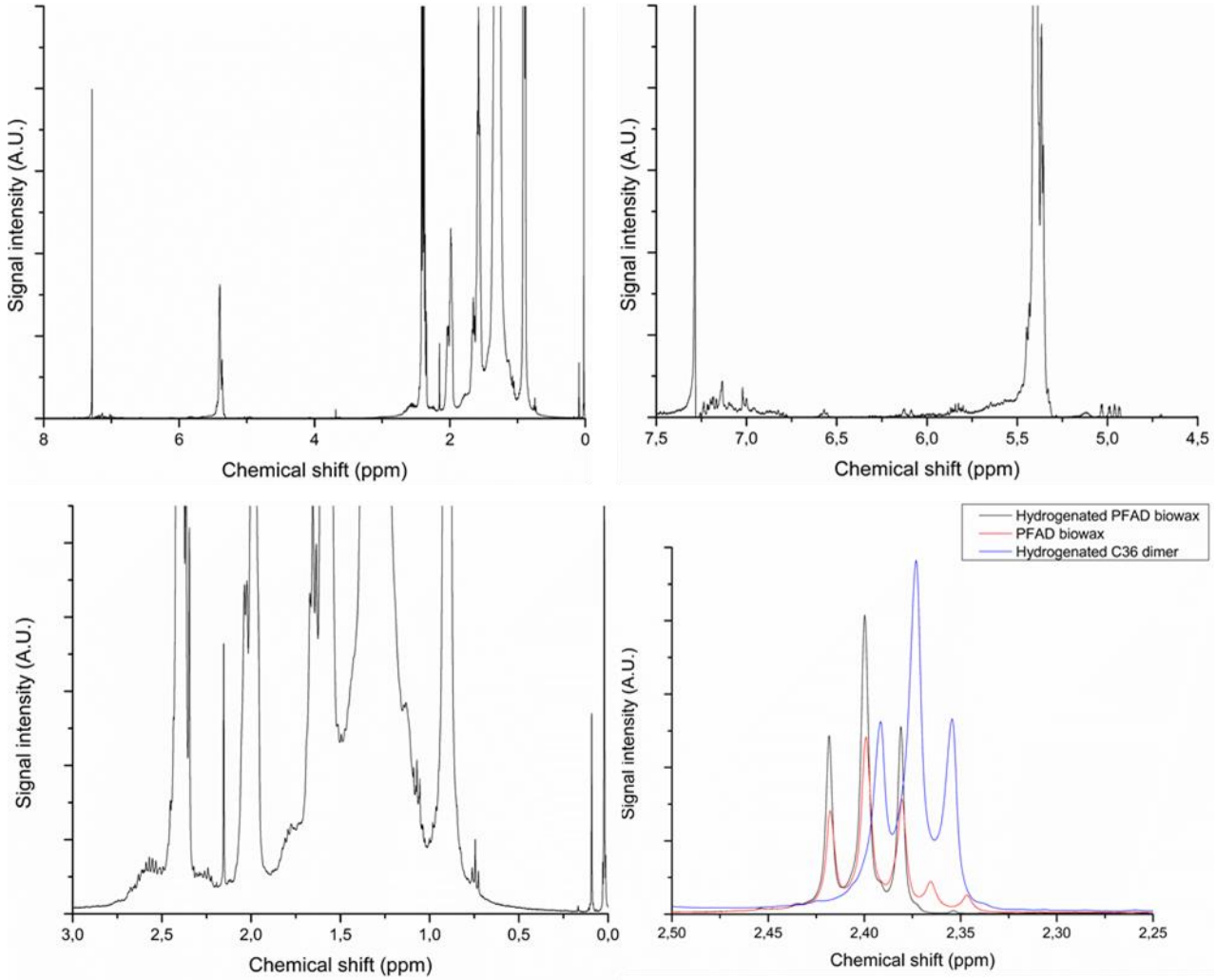

Figure S15: ^{1}H-NMR analysis of the crude PFAD bio-wax, including comparison with its hydrogenated counterpart and commercia C_{36} dimer acids.

In contrast, the ^{1}H-NMR spectrum of the hydrogenated PFAD bio-wax does not contain these specific signals which are characteristic for the presence of unsaturated fatty acid dimers/trimers (Figure S16). The main ketone triplet is clearly visible, while some small signals corresponding to the presence of trace amounts of unsaturation are observed. This is due to the fact that the initial hydrogenation reaction resulted in 97% saturated feedstock, with 3% residual oleic acid before ketonization.

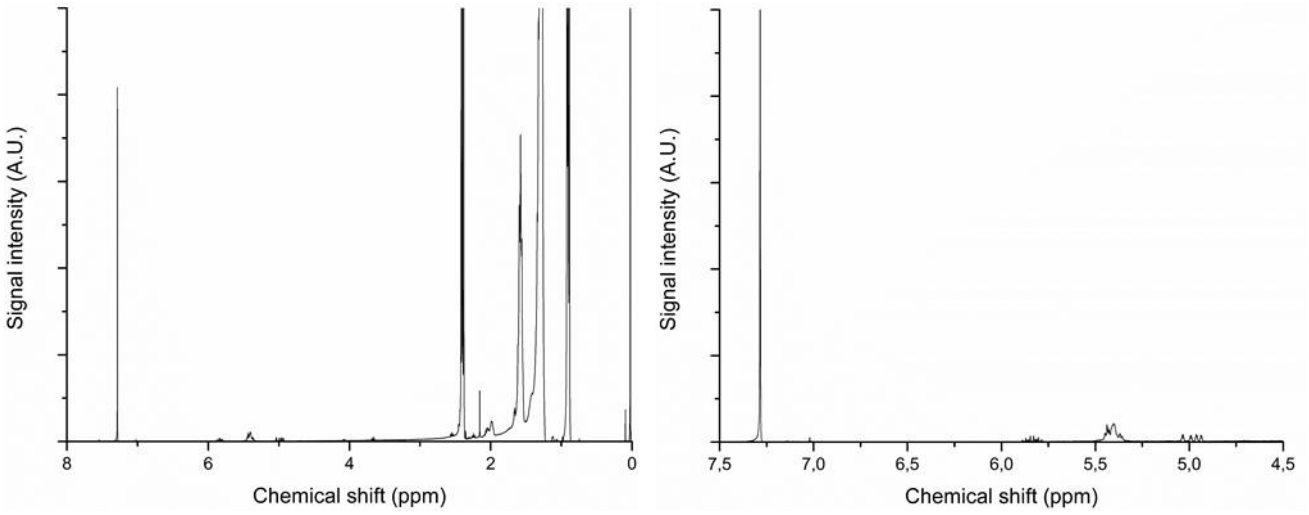

Figure S16: ^{1}H-NMR analysis of the bio-wax originating from hydrogenated PFAD substrate.

Differential scanning calorimetry. The melting point and heat capacity of the PFAD biowax were determined by differential scanning calorimetry (DSC) analysis (Figure S17). The melting point peak is situated around 71°C, while the overall melting profile is broad between approximately 55-75°C. The measured average heat capacity of the liquid wax product was 3.28 J/g.K between 80-100°C (above melting point).

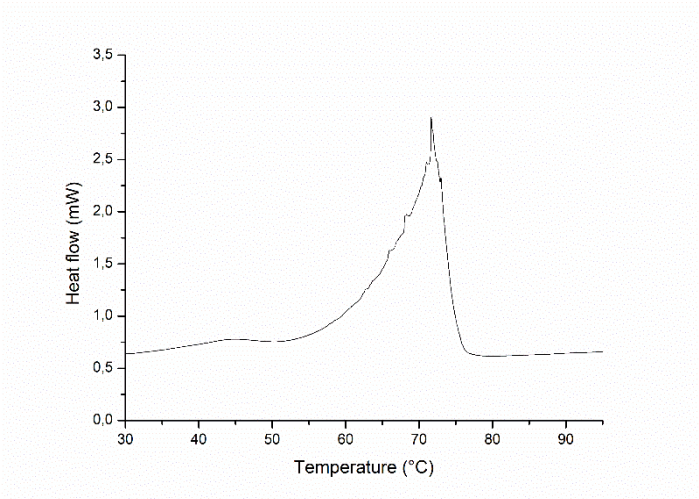

Figure S17: Differential scanning calorimetry of PFAD bio-wax product (endo up).

4. Application of ketone bio-waxes

Ketonization of other commercial fatty acid feedstock. Animal fat (59% FFA and 41% triglycerides, by-product of chemical animal fat refining) and coconut and palm kernel fatty acids were used as ketonization substrates to produce ketone bio-waxes (Table S1). After full fatty acid conversion, the coconut and palm kernel derived bio-waxes consisted of around 97 and 96% ketones respectively, mainly comprised of saturated C_{23}-C_{27} ketones. For the animal product, no free fatty acids were present in the bio-wax and the ketone yield was 61% with 1% C_{15}-C_{17} hydrocarbons. The remaining fraction was not detectable by GC(-MS) analysis, and most likely unconverted triglycerides and dimers/trimers.

Table S1: Starting free fatty acid composition and final bio-wax ketone distribution of different commercial fatty acid feedstock (in wt%).

Substrate	Animal	Coconut	Palm Kernel	Product	Animal	Coconut	Palm Kernel
Lauric acid	0	54	50	**C23**	0	38	34
Myristic acid	1	19	17	**C25**	0	24	23
Palmitic acid	16	12	9	**C27**	0	16	14
Stearic acid	9	2	3	**C29**	1	13	17
Oleic acid	33	11	18	**C31**	14	3	5
Linoleic acid	0	2	3	**C33**	23	2	2
Triglycerides	41	/	/	**C35**	23	1	1
				C_{15}-C_{17} hydrocarbons	1	<1	<1
				Dimers/trimers	N.D.	4	5
				Triglycerides	N.D.	/	/

N.D.: Not determined

Differential scanning calorimetry. The melting point of the palm kernel derived bio-wax was determined by differential scanning calorimetry (DSC) analysis (Figure S18). The melting point peak is situated around 53 °C, while the overall melting profile is broad between 40-55 °C.

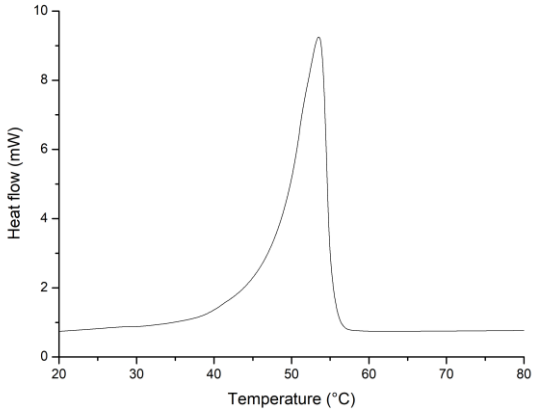

Figure S18: Differential scanning calorimetry of palm kernel bio-wax ketone product (endo up).

Thermogravimetric analysis. The thermal stability of several compounds was determined under oxidative conditions (O_2) via TGA up to 750 °C (Figure S19). For most samples, the primary weight loss starts to occur at the onset temperature of around 200 °C, with exception of the PFAD substrate and commercial C_{36} dimer acid mixture. For the PFAD bio-wax and dimer acids, significant weight loss still occurs between 300-500 °C.

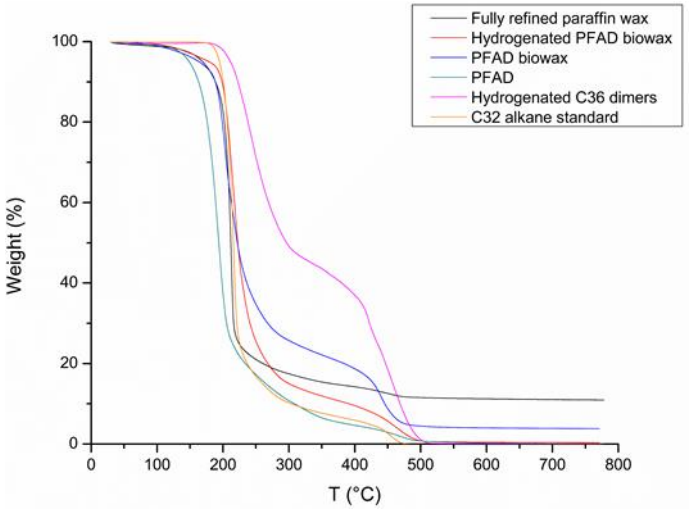

Figure S19: TGA profiles of ketone bio-waxes and related compounds.

5. Process design

Palmitic acid vapour pressure calculation. The Clausius-Clapeyron equation was used to determine the boiling point of pure palmitic acid at 10 bar. When we assume that the enthalpy of vaporization ΔH_{vap} has a constant value of 97.5 kJ/mol in the relevant temperature range, and the normal boiling point (at 1 atm.) of pure palmitic acid is 350 °C[15] , then the boiling point of palmitic acid is around 437 °C at 10 bar. Therefore, under ketonization conditions (350 °C), the vapour pressure of palmitic acid was calculated as 10 kPa.

$$\ln\left(\frac{P_1}{P_2}\right) = -\frac{\Delta H_{vap}}{R}\left(\frac{1}{T_1} - \frac{1}{T_2}\right)$$

Inventory data. Table S2 contains a detailed overview of the inventory data and description of the accompanying assumptions that were made to compose the overall mass and energy balances of the PFAD ketonization process. A batch size of 3656 kg PFAD was selected (assuming 345 net production days per year and 4 ketonization reactions per day in two 4.3 m³ reactors). Physico-chemical properties such as liquid viscosity and heat capacity were determined for the feedstock and/or substrate in order to calculate the required thermal and electrical power consumption during the heating and pumping operations. The endothermic standard enthalpy of reaction is 30 kJ/mol for palmitic acid ketonization[16]. The enthalpy of reaction at 350 °C was estimated based on the estimated temperature dependence of the heat capacities of substrates and products.[17]. To determine the energy consumption of an industrial disk stack centrifuge for this application, both estimated data using an upscaling framework[18] and published values of manufacturers are similar and in the order of magnitude between 30-50 kWh. Based on the lab scale results and industry expertise, the amount of catalyst loss for this step was set at 3%, with a product loss of 1%. Regarding the efficiency of the proposed technologies, values of 85 and 40% were assumed for heating and pumping steps, respectively (based on multiple discussion with industrial engineering experts). Finally, also the heating capacity of the reactor and storage vessels were taken into account, and for all pumping and storage steps a temperature loss of 2°C is assumed and accounted for in the overall energy balance.

Table S2: Inventory data for PFAD ketonization process scheme.

Parameter	Value	Description
Process duty		
Wax output per year	5 kiloton	
Net production days per year	345	20 maintenance days per year are included
Batch/year	1380	Batch time is 6 hours
Batch size	3656 kg	
Reactor size	4.3 m^3	2 reactors are used sequentially
PFAD Substrate		
Liquid viscosity at 100°C	0.0044 Pa.s	Measured in this work and assumed constant
Average molecular weight	268 g/mol	Based on fatty acid composition
Average heat capacity	2.8 J/gK	Estimated average between 15-350°C[17]
Density at 25°C	878 kg/m^3	Based on literature[19]
Ketonization reaction		
Standard reaction enthalpy at 25°C	30 kJ/mol	For pure palmitic acid ketonization[16]
Reaction enthalpy at 350°C	55 kJ/mol	Estimation based on literature[17, 20]
Wax product		
Liquid viscosity at 100°C	0.0061 Pa.s	Measured in this work and assumed to be constant
Average molecular weight	510 g/mol	For the dimer/trimer side products an average MW of 700 g/mol was chosen
Average heat capacity 80-100°C	3.28 J/gK	Measured in this work and assumed to be constant in temperature range
TiO_2 catalyst		
Loading	5 wt%	For fresh catalyst in first run, based on lab scale results
Centrifugation		
Energy consumption	30-50 kWh	Based on literature[18] and discussion with industry expert
Catalyst loss	3%	Based on lab scale results and discussion with industry expert
Product loss	1%	
Other process parameters		
Heating/cooling efficiency	85%	
Pump efficiency	40%	
Heat capacity reactor and storage vessels	0.52 J/gK	
Heat loss during storage/pumping	2°C	

Reaction enthalpy and energy requirement. Figure S20 depicts the overall energy requirement of the PFAD ketonization process for one batch as a function of the reaction enthalpy at 350 °C. The standard enthalpy of reaction for pure palmitic acid is around 30 kJ/mol[16], whereas 55 kJ/mol was calculated as the estimated value at 350 °C due to the temperature dependence of the heat capacity of feedstock and products. For this, average heat capacity values were estimated between 25-350°C.[17, 20]

$$\Delta H_r(623\ K) = \Delta H_r(298\ K) + \Delta C_p \Delta T$$

$$H_r(298\ K) = \frac{30kJ}{mol}$$

$$\Delta T = 325K$$

$$\Delta C_p = C_{p,ketone} + C_{p,H2O} + C_{p,CO2} - 2C_{p,acid}$$

$$C_{p,ketone} = 1.37\frac{kJ}{mol.K}$$

$$C_{p,H2O} = 0.075\frac{kJ}{mol.K}$$

$$C_{p,CO2} = 0.041\frac{kJ}{mol.K}$$

$$C_{p,acid} = 0.70\frac{kJ}{mol.K}$$

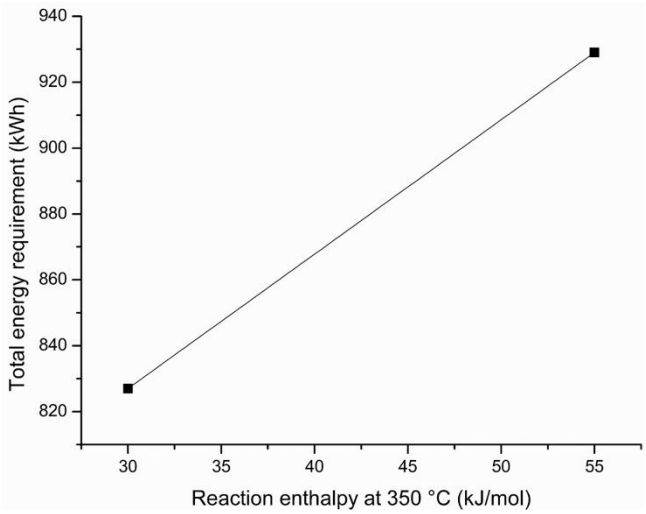

Figure S20: Impact of ketonization reaction enthalpy of PFAD at 350 °C on the total energy requirement of 1 batch.

Estimation of bio-wax production price. In Table S3, an overview of the required process inputs is provided over the course of 3 batches, alongside their respective unit prices to calculate an estimated bio-wax product cost. The deactivation profile of the catalyst over 3 runs was taken into account. Starting from 5 wt% of fresh catalyst in the first run (183 kg), fresh catalyst has to be added for batches 2 and 3 to achieve full conversion. In total, 9855 kg of bio-wax is produced from 10,970 kg PFAD feedstock and 290 kg TiO_2 catalyst over 3 batches. These calculations also incorporated the 1% product and 3% catalyst losses per batch. Regarding the catalyst separation via centrifugation, a cost of around €29 per run was calculated (€25,000 yearly CAPEX cost over 20 years + €5,000 yearly maintenance + €2,000 operating cost for electricity and water). Figure S21 shows the impact of a variable TiO_2 price on the overall bio-wax cost, under the assumption that the other input prices remain constant.

Table S3: Estimation of bio-wax product cost based on mass inputs and associated prices for 3 consecutive batches.

Input	Quantity per 3 batches	Input price per unit (€)	Price per 3 batches (€)	Price per ton bio-wax (€)
PFAD	10.97 ton	600[21, 22]	6582	668
N_2	0.600 ton	102[23]	61	6
TiO_2	0.290 ton	1000-15000	290-4350	29-441
Catalyst separation*	3 runs	29	87	9
Thermal energy	2340 kWh	0.03[24]**	70	7
Electricity	447 kWh	0.1[25]	45	5
Total			**7135-11195**	**724-1136**

* Thermal energy costs of this step is incorporated in row 5.

** Average non-household natural gas price per kWh in EU for 2019, source: Eurostat.

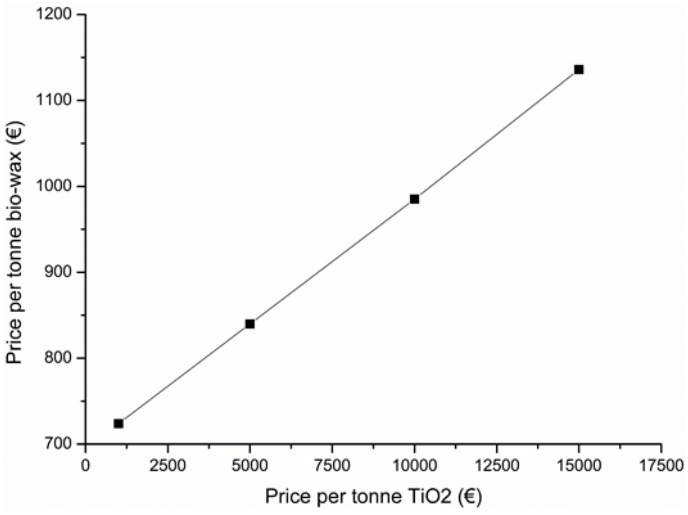

Figure S21: Impact of TiO_2 catalyst price on the total ketone bio-wax manufacturing cost.

6. Life cycle assessment

Base case life cyle inventory. Table S4 represents the overall mass balance of the PFAD ketonization process for 3 large scale batches, including the necessary amount of catalyst and N_2 for full conversion of the biomass feedstock. The total input is higher than the total output due to the small product and catalyst losses of the process.

Table S4: Mass inventory for 3 batches PFAD conversion in the TiO_2 catalysed ketonization process.

Input	Quantity (kg)	Output	Quantity (kg)
PFAD	10 968	Bio-wax	9855
N_2	600	H_2O	264
TiO_2	290	CO_2	645
		Trace gasses	18
		N_2	600
		TiO_2	276
Total input	**11858**	**Total output**	**11658**

Economic allocation calculation. The production of 1 functional unit requires 1.11 kg of PFAD feedstock. Palm fatty acid distillate is a 4.5 wt% by-product of the crude palm oil refining process. In this study, market prices of €600 and €770 were used per ton of PFAD and refined palm oil (RPO), respectively.[21, 22] This leads to an economic allocation factor of 3.41% for PFAD (Table S5). Based on these calculations, the impact modelling factor for 1 FU in Gabi software with reference to RPO is 84.1 % (= $3.41\% * 24.67$).

Table S5: Determination of economic allocation factors for refining of crude palm oil to PFAD and refined palm oil.

	Output stream i	Mass m_i (kg)	Price p_i (€/kg)	$m_i * p_i$ (€)	Economic allocation factor (%) $\frac{m_i * p_i}{\sum m_i * p_i}$
Production of 1.11 kg PFAD (= 1 FU)	**PFAD**	**1.11**	**0.60**	**0.67**	**3.41**
	RPO	**24.67**	**0.77**	**18.99**	**96.59**

Detailed breakdown of paraffin wax climate change impact. In Figure S22, the carbon footprint of paraffin wax is broken down into its main constituents. The net CCI equals 2.83 kg CO_2 eq./FU, of which 1.09 kg CO_2 eq./FU originates from the paraffin production process. The end-of-life incineration is the largest contributor with 3.13 kg CO_2 eq./FU, although significant amounts of electricity (-0.69 kg CO_2 eq./FU) and thermal energy (-0.71 kg CO_2 eq./FU) can be recovered during this step, reducing the net overall carbon footprint.

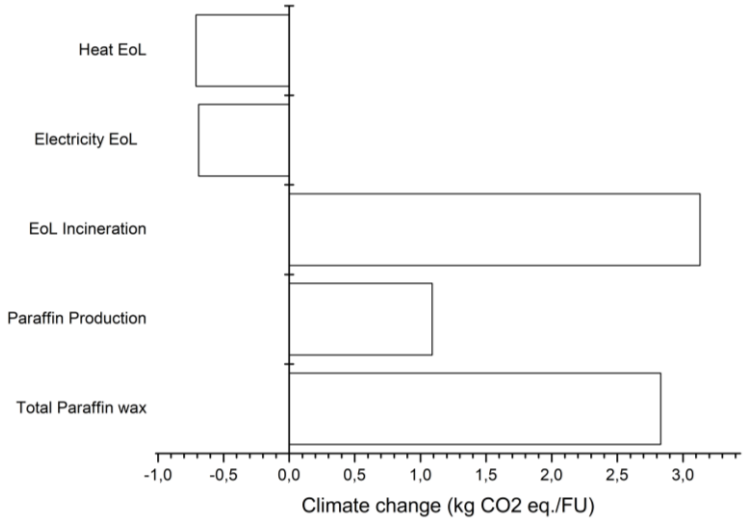

Figure S22: Detailed breakdown of the climate change impact (CCI) of paraffin wax.

Comparison of LUC emissions for top 20 palm oil producers. In Table S6, the LUC emissions for natural vegetation to palm oil cultivation and weighted global average emissions are shown based on FAO 2008 yield data for the top 20 palm oil producers by country.

Table S6: LUC emissions for natural vegetation to palm oil by country for top 20 producers and weighted global average emissions based on FAO 2008 yield data.[9]

Country	Average LUC emissions (ton CO_2 eq. ha^{-1} $year^{-1}$)	Annual yield (ton oil ha^{-1})	LUC emissions (ton CO_2 eq. ton oil^{-1})	Contribution to weighted global average % ton CO_2 eq.	
Malaysia	27.9	4.5	6.1	43.4	2.7
Indonesia	26.9	3.4	8.0	41.3	3.3
Nigeria	11.5	4.2	2.8	3.3	0.1
Thailand	8.1	2.8	2.9	3.2	0.1
Colombia	16.3	4.7	3.5	1.9	0.1
Papua New Guinea	25.2	4.0	6.3	0.9	0.1
Ecuador	13.9	2.3	6.1	0.8	<0.1
Ivory Coast	21.0	1.35	15.6	0.7	0.1
Honduras	16.1	2.9	5.5	0.7	<0.1
China	4.6	4.7	1.0	0.6	<0.1
Brazil	17.3	3.3	5.2	0.5	<0.1
Costa Rica	17.1	3.7	4.6	0.5	<0.1
Cameroon	17.7	3.1	5.6	0.5	<0.1
Guatemala	15.0	3.7	4.1	0.5	<0.1
DR Congo	21.9	1.0	21.0	0.4	0.1
Ghana	17.9	0.4	47.1	0.3	0.1
Venezuela	14.0	3.3	4.2	0.2	<0.1
Philippines	25.1	3.7	6.7	0.2	0.1
Mexico	10.5	0.3	40.4	0.2	0.1
Guinea	17.0	0.2	105.6	0.1	0.1
Global weighted average LUC emissions (ton CO_2 eq. ton oil^{-1})					7.0

POME Treatment. Biogenic methane emissions have been tracked and used for thermal energy production from the captured biogas (0.017 kg of biogenic methane is emitted during production of 1 kg PFAD). It is assumed that the biogas consists of 100% of the methane released from open pond POME treatment and from the anaerobic decomposition of by-products such as empty fruit bunches and palm kernels. It must be noted that for the base case scenario of this study, only 5% of these POME methane emissions were modelled for usage as a biogas energy source, as stated in the experimental section. Regarding energy recuperation, 100% efficiency was assumed. Although this value will be slightly lower in a practical application, it will still produce a valid scenario as more than 99% of the impact reduction originates from the avoided methane emissions (and only to a minor extent from the recovered energy).

Calculation of CCI of PFAD hydrogenation. The additional CCI of hydrogenation was calculated based on additional impacts of thermal energy required, as well as the impacts of H_2 and the hydrogenation catalyst (Table S7). Regarding thermal energy requirements, the substrate has to be heated up to 210 °C, while no additional heating is required during reaction due to the exothermic nature of the hydrogenation reaction. This is in contrast with the endothermic ketonization reaction. We have set this impact value equal to that corresponding to heating to 350 °C for the ketonization reaction (0.02 kg CO_2 eq./FU), avoiding any underestimation. Taking into account the chemical composition of PFAD, 3.86 g H_2 is required to fully hydrogenate 1 kg PFAD. Depending on the hydrogen source, the CCI of H_2 ranges from 0.97 (using renewable energy) to 31 (using electricity grid) kg CO_2 equivalent for 1 kg H_2 production by electrolysis. The CCI of 1 kg H_2 production by steam reforming ranges from 1.75 (steam cracker) to 11.8 (steam reforming of natural gas) kg CO_2 equivalent.[25-28] Based on these numbers, an average value of 16 kg CO_2 eq./kg H_2 was selected, resulting in an average value of 0.07 kg CO_2 eq./FU. The impact of the hydrogenation catalyst was set equal to that of the required hydrogen to avoid underestimation. Our group has previously shown that the impact of a similar hydrogenation catalyst (64% Ni/SiO_2) is significantly lower than the CCI of H_2 during fractionation and hydroprocessing reactions of lignin to phenols (impact for nickel (99.5%) was 0,000236 kg CO2 eq/kg phenol).[25]

Table S7: Overview of CCI of inputs for PFAD hydrogenation.

Input	CCI (kg CO_2 eq./FU)
Thermal energy	0.02
H_2	0.07
Hydrogenation catalyst	0.07
Total	**0.16**

Scenario analysis of bio-wax lifetime. In Figure S23, the CCI of bio-wax was calculated for bio-wax lifetimes ranging between 10-200% compared to the lifetime of paraffin wax. The respective carbon footprint values range between 29.4-1.47 kg CO_2 eq./FU, with the CCI of paraffin wax at constant 2.83 kg CO_2 eq./FU.

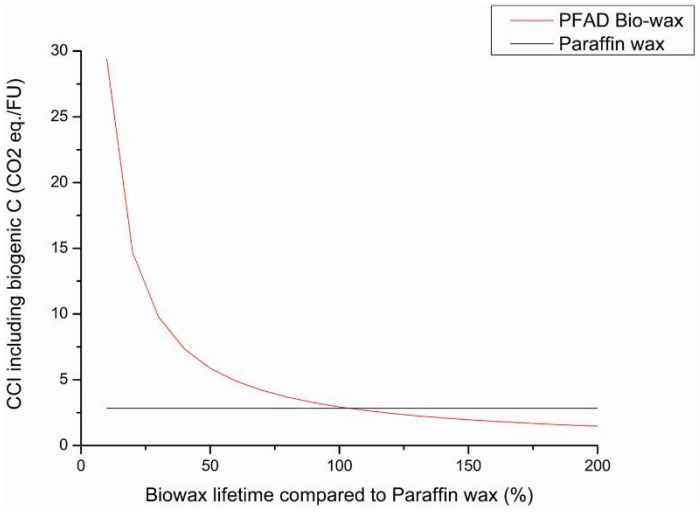

Figure S23: Scenario analysis of CCI of bio-wax for product lifetimes ranging between 10-200% compared to paraffin wax.

Carbon footprint of ketone bio-waxes originating from other fatty acid feedstock. Literature data were used to calculate predicted CCI values of other ketone bio-waxes synthesized by our process.[29, 30] For this, it is assumed that the same amount of fatty acid substrate is required for the production of 1 FU (1 kg bio-wax) as in our base PFAD LCA study. This implies that the bio-waxes can be produced in similar yields for all substrates, which is supported by our experiments carried out on the other fatty acids in section 3.5. The difference in the amount of unsaturation in these substrates is not a significant differentiating factor, as their hydrogenation to saturated oils and fatty acids is a readily available and established oleochemical process. As we have shown in our scenario analysis, the hydrogenation step is not a major contributor to the overall CCI. Furthermore, triglyceride hydrolysis is similar for these feedstocks, and no significant contributor to the overall CCI of the fatty acids.[31]

References

1. Thinkstep, “Process data set: Wax /Paraffins at refinery; from crude oil; production mix, at refinery; 38 MJ/kg net calorific value (en).”. 2018.
2. Thinkstep, “Process data set: Palm oil, refined (incl. LUC as fossil CO2); technology mix; production mix, at plant; refined (en),”. 2018.
3. Analytics, P. O., “Essential Palm Oil Statistics 2017.”. 2017.
4. Sea-distances.org "Port-to-port distance: Pasir Gudang to Rotterdam.”. https://sea-distances.org/ (accessed 04.30.2019).
5. WorldAtlas “Top Palm Oil Producing Countries In The World - WorldAtlas.com.”. https://www.worldatlas.com/articles/top-palm-oil-producing-countries-in-the-world.html (accessed 11.28.2018).
6. OEC “OEC - Import origins of Palm Oil to Belgium-Luxembourg (2017)”. https://atlas.media.mit.edu/en/visualize/tree_map/hs92/import/blx/show/1511/2017/ (accessed 04.08.2019).
7. OEC "OEC - Import origins of Palm Oil to the Netherlands (2017)”. (accessed 04.08.2019).
8. Abdul Kapor, N. Z.; Maniam, G. P.; Rahim, M. H. A.; Yusoff, M. M., Palm fatty acid distillate as a potential source for biodiesel production-a review. *Journal of Cleaner Production* **2017,** *143*, 1-9.
9. Flynn, H. C.; Canals, L. M. i.; Keller, E.; King, H.; Sim, S.; Hastings, A.; Wang, S.; Smith, P., Quantifying global greenhouse gas emissions from land-use change for crop production. *Global Change Biology* **2012,** *18* (5), 1622-1635.
10. Time, G.; Isic, S., "Ecoinvent 3.3 dataset documentation on titanium dioxide production, sulfate process for Europe.". 2005.
11. Maheu, C.; Cardenas, L.; Puzenat, E.; Afanasiev, P.; Geantet, C., UPS and UV spectroscopies combined to position the energy levels of TiO2 anatase and rutile nanopowders. *Physical Chemistry Chemical Physics* **2018,** *20* (40), 25629-25637.
12. Barreau, M.; Courtois, X.; Can, F., FT-IR spectroscopy study of HNCO adsorption and hydrolysis over oxide-based samples dedicated to deNOx processes. *Applied Catalysis A: General* **2018,** *552*, 147-153.
13. Tamura, M.; Shimizu, K.-i.; Satsuma, A., Comprehensive IR study on acid/base properties of metal oxides. *Applied Catalysis A: General* **2012,** *433-434*, 135-145.
14. Park, K. J.; Kim, M.; Seok, S.; Kim, Y.-W.; Kim, D. H., Quantitative analysis of cyclic dimer fatty acid content in the dimerization product by proton NMR spectroscopy. *Spectrochimica Acta Part A: Molecular and Biomolecular Spectroscopy* **2015,** *149*, 402-407.
15. Stephenson, R. M.; Malanowski, S., *Handbook of the Thermodynamics of Organic Compounds*. 1987.
16. Kanervo, J.; Toppinen, S.; Nurmi, P. Method For Producing Ketones For Fuel And Oil Applications. US 2019/0185759 A1, 2018/12/17, 2019.
17. Cedeño, F. O.; Prieto, M. M.; Xiberta, J., Measurements and Estimate of Heat Capacity for Some Pure Fatty Acids and Their Binary and Ternary Mixtures. *Journal of Chemical & Engineering Data* **2000,** *45* (1), 64-69.
18. Piccinno, F.; Hischier, R.; Seeger, S.; Som, C., From laboratory to industrial scale: a scale-up framework for chemical processes in life cycle assessment studies. *Journal of Cleaner Production* **2016,** *135*, 1085-1097.
19. Top, A., Production and utilization of palm fatty acid distillate (PFAD). *Lipid Technology* **2010,** *22*, 11-13.
20. Nakasone, K.; Takamizawa, K.; Shiokawa, K.; Urabe, Y., Simultaneous determination of the heat capacity and the heat of the transitions for long-chain compounds with a heat-flux type DSC. *Thermochimica Acta* **1994,** *233* (2), 175-185.
21. The World Bank World Bank Commodities Price Data. http://pubdocs.worldbank.org/en/520721601663433090/CMO-Pink-Sheet-October-2020.pdf (accessed August 2020).
22. Malaysian Palm Oil Board Prices of selected oils and fats (North-West Europe Market US$/Tonne) - 2020. http://bepi.mpob.gov.my/index.php/en/?option=com_content&view=article&id=906&Itemid=138 (accessed September 2020).
23. Tschulkow, M.; Compernolle, T.; Van den Bosch, S.; Van Aelst, J.; Storms, I.; Van Dael, M.; Van den Bossche, G.; Sels, B.; Van Passel, S., Integrated techno-economic assessment of a biorefinery process: The high-end valorization of the lignocellulosic fraction in wood streams. *Journal of Cleaner Production* **2020,** *266*, 122022.
24. Eurostat Gas prices for non-household consumers - bi-annual data (from 2007 onwards). https://ec.europa.eu/eurostat/databrowser/view/nrg_pc_203/default/table?lang=en (accessed September 2020).
25. Liao, Y.; Koelewijn, S.-F.; Van den Bossche, G.; Van Aelst, J.; Van den Bosch, S.; Renders, T.; Navare, K.; NicolaГЇ, T.; Van Aelst, K.; Maesen, M.; Matsushima, H.; Thevelein, J. M.; Van Acker, K.; Lagrain, B.; Verboekend, D.; Sels, B. F., A sustainable wood biorefinery for lowвЂ“carbon footprint chemicals production. *Science* **2020,** *367* (6484), 1385-1390.
26. Cetinkaya, E.; Dincer, I.; Naterer, G. F., Life cycle assessment of various hydrogen production methods. *International Journal of Hydrogen Energy* **2012,** *37* (3), 2071-2080.
27. Bhandari, R.; Trudewind, C. A.; Zapp, P., Life cycle assessment of hydrogen production via electrolysis – a review. *Journal of Cleaner Production* **2014,** *85*, 151-163.

28. Marquevich, M.; Sonnemann, G. W.; Castells, F.; Montané, D., Life cycle inventory analysis of hydrogen production by the steam-reforming process: comparison between vegetable oils and fossil fuels as feedstock. *Green Chemistry* **2002,** *4* (5), 414-423.
29. Schmidt, J. H., Life cycle assessment of five vegetable oils. *Journal of Cleaner Production* **2015,** *87*, 130-138.
30. Schowanek, D.; Borsboom-Patel, T.; Bouvy, A.; Colling, J.; de Ferrer, J. A.; Eggers, D.; Groenke, K.; Gruenenwald, T.; Martinsson, J.; McKeown, P.; Miller, B.; Moons, S.; Niedermann, K.; Pérez, M.; Schneider, C.; Viot, J.-F., New and updated life cycle inventories for surfactants used in European detergents: summary of the ERASM surfactant life cycle and ecofootprinting project. *The International Journal of Life Cycle Assessment* **2018,** *23* (4), 867-886.
31. Tufvesson, L. M.; Börjesson, P., Wax production from renewable feedstock using biocatalysts instead of fossil feedstock and conventional methods. *The International Journal of Life Cycle Assessment* **2008,** *13* (4), 328.